Intermetallics 18 (2010) 1544–1552

Contents lists available at ScienceDirect

Intermetallics

journal homepage: www.elsevier.com/locate/intermet

Phase fractions, transition and ordering temperatures in TiAl–Nb–Mo alloys: An in- and ex-situ study

Thomas Schmoelzer [a,*], Klaus-Dieter Liss [b], Gerald A. Zickler [c], Ian J. Watson [b], Laura M. Droessler [a], Wilfried Wallgram [d], Thomas Buslaps [e], Andrew Studer [b], Helmut Clemens [a]

[a] Department Physical Metallurgy and Materials Testing, University of Leoben, Franz-Josef-Straße 18, A-8700 Leoben, Austria
[b] Australian Nuclear Science and Technology Organisation, PMB 1, Menai NSW 2234, Australia
[c] Christian Doppler Laboratory for Early Stages of Precipitation, Department Physical Metallurgy and Materials Testing, University of Leoben, Franz-Josef-Straße 18, A-8700 Leoben, Austria
[d] Böhler Schmiedetechnik GmbH&Co KG, Mariazellerstraße 25, A-8605 Kapfenberg, Austria
[e] European Synchrotron Radiation Facility (ESRF), Polygone Scientifique Louis Néel, 6 rue Jules Horowitz, F-38000 Grenoble, France

ARTICLE INFO

Article history:
Received 23 December 2009
Received in revised form
8 April 2010
Accepted 14 April 2010
Available online 8 May 2010

Keywords:
A. Titanium aluminides, based on TiAl
B. Alloy design
B. Order/disorder transformations
B. Phase transformations
C. Heat treatment
F. Diffraction

ABSTRACT

Intermetallic γ-TiAl based alloys of the TNM™ alloy family attain their excellent processing characteristics by a high β-phase content present at hot-working temperatures. Subsequent to hot-working the β-phase content is decreased by a heat treatment step performed at temperatures where the β-phase fraction exhibits a minimum. In this study, in- and ex-situ experiments were conducted on three alloys with different contents of β/β_0 stabilizing elements. The course of phase fractions as a function of temperature as well as phase transition temperatures were determined by means of in-situ high-energy X-ray diffraction experiments. Additionally, dynamic scanning calorimetry investigations were performed to obtain complementary data on the transition temperatures. Quantitative metallography was conducted on heat treated and quenched specimens to acquire additional information on the dependence of the phase fractions on temperature. By neutron diffraction experiments the ordering temperatures of the constituent phases were determined. It was shown that the experiments yielded consistent results which differ significantly from ThermoCalc simulations for which a commercial TiAl database was used. The differences between the experimental results and the thermodynamic predictions are discussed.

1. Introduction

Intermetallic γ-TiAl based alloys are believed to have great potential in high temperature applications, mainly due to their high specific tensile and creep strength at elevated temperatures [1–3]. One of the reasons why this material class has not found widespread application yet are the difficulties associated with its processing [4]. Conventional high Nb bearing γ-TiAl alloys, which show only a small volume fraction of β-phase at hot-working temperature [5], can only be forged under isothermal conditions, which is not economically feasible for most applications [6]. Therefore, the development of alloys that can be processed by near conventional forging operations is an important step towards the mass production of TiAl parts.

So-called TNM™ alloys are among the most promising candidates to meet this requirement. This name is derived from Nb and Mo which are the decisive alloying elements. The overall composition of these alloys is in the range of Ti – (42–45) Al – (3–5) Nb – (0.1–2) Mo – (0.1–0.2) B (in at%) [4]. It has been proven that good processing characteristics are achieved by high β-phase contents at hot-working temperatures [4,6,7]. The presence of the disordered bcc β-phase is beneficial to the deformation behaviour because dislocation motion as well as dynamic recrystallization is easily facilitated in this phase [8–10]. At service temperature (600–750 °C) the β-phase shows an ordered B2-structure, which is termed β_0 in the following. To avoid the adverse effect of high β_0-phase contents on creep behaviour and room-temperature ductility [11–13], efforts were made to design alloys in a way that allows to minimize the remaining β_0-phase fraction by special two-step heat treatments after forging [4,7,14].

One requirement for the realization of this approach is the existence of low equilibrium β/β_0-phase fractions at temperatures

* Corresponding author. Tel.: +43 3842 4024267; fax: +43 3842 4024202.
E-mail address: thomas.schmoelzer@unileoben.ac.at (T. Schmoelzer).

0966-9795/$ – see front matter © 2010 Elsevier Ltd. All rights reserved.
doi:10.1016/j.intermet.2010.04.008

high enough to attain equilibrium conditions rather rapidly. The first step of the heat treatment is performed to reduce the β/$β_0$-phase fraction to the desired level. After the second heat treatment step, which is conducted well below the eutectoid temperature, the microstructure consists of three prominent phases: (a) γ-TiAl exhibiting an ordered tetragonal $L1_0$-structure, (b) $α_2$-Ti_3Al showing a $D0_{19}$ structure which disorders at the eutectoid temperature to an unordered hcp-structure and (c) the $β_0$-phase with B2 structure which disorders at elevated temperatures to bcc β-phase. For details concerning the alloy design strategy, hot working behaviour, heat treatments, and mechanical properties the reader is referred to [4,7,12,15,16].

To design an alloy that exhibits the above described behaviour, thermodynamic calculations were performed for alloys containing different amounts of the β/$β_0$-stabilizing elements Mo and Nb [4]. This study was conducted by employing the CALPHAD (CALculation of PHAse Diagrams) method, using a commercially available database [17]. The results of this investigation are summarized in Fig. 1. Clemens et al. [12] demonstrated that all alloy variants solidify via the β-phase. From comparison of the evolution of phase fractions in the alloys termed A, B, and C it is obvious that Mo is a stronger β/$β_0$ stabilizer than Nb, which is in agreement with the results of other studies [18,19].

Furthermore, for all three alloys the thermodynamic calculations show a local minimum of the $β_0$-phase mole fraction at around 1275 °C. Above this temperature the fraction of $β_0$-phase strongly increases with temperature. However, at the temperature where the minimum in $β_0$-phase appears, Ti-43.5Al-4Nb-1Mo-0.1B (Alloy A) shows the smallest fraction of $β_0$-phase. By increasing the amount of Nb or Mo by 1 at% or 0.5 at%, respectively, the mole fraction of the $β_0$-phase in its minimum is considerably increased. Below 1275 °C the $β_0$-fraction slightly increases with decreasing temperature (Fig. 1a; alloy A) or shows an approximately constant value (Fig. 1b and c; alloys B and C). At temperatures lower than the eutectoid temperature (~1115 °C) the $β_0$-phase fraction decreases with decreasing temperature for all three alloys. From the phase predictions displayed in Fig. 1 it is obvious that none of the three alloys exhibit a single phase region at temperatures below 1400 °C.

Since the thermodynamic database [17] used for the Thermo-Calc calculations is not well suited for describing the behaviour of highly alloyed TiAl-systems [5,20,21], doubt has been cast on the reliability of the results obtained by the thermodynamic simulations shown in Fig. 1. Furthermore, the simulation predicted that the ordered $β_0$-phase is stable up to temperatures as high as 1420 °C [16]. In contrast to that, non-isothermal hot-forging tests conducted on industrial-scale equipment showed that alloys with comparable composition exhibit good deformation behaviour at temperatures well below 1400 °C [4,7]. Since ordered $β_0$ shows higher deformation resistance than disordered β, the validity of the predicted ordering temperature was questioned [22,23].

In the light of these findings, it has been established that thermodynamic predictions as shown in Fig. 1 yield trends rather than accurate values of the phase fractions and transition temperatures [16,21]. Although the calculations are performed for equilibrium conditions, recent investigations indicate that the results of thermodynamic calculations reflect the materials behaviour observed in short-time annealing experiments [21]. Evidence for this assertion was obtained from differential scanning calorimetry (DSC) investigations and long-term annealing experiments which have revealed the existence of an α-single-phase field that was not predicted by the ThermoCalc simulations shown in Fig. 1 and was not observed at moderate annealing times. However, understanding the phase equilibria and transition temperatures of the investigated alloy system is a prerequisite for performing hot-working operations and for defining appropriate heat treatment parameters.

A thorough knowledge of the constituent phase fractions and their dependence on temperature and time are, therefore, crucial for the present and further development of the investigated alloys. In this study, a number of complementary experiments were conducted to investigate how accurate the predictions of the thermodynamic calculations shown in Fig. 1 are. The dependence of the phase fractions on temperature was determined by means of in- and ex-situ methods. During continuous heating the evolution of phase fractions was monitored by in-situ high energy synchrotron X-ray diffraction (HEXRD). Applications and techniques concerning HEXRD experiments can be found in [24–27]. DSC experiments were carried out to verify the transformation temperatures obtained by HEXRD. Additionally, annealing experiments at elevated temperatures followed by rapid air cooling were conducted to analyse the phase fractions by a metallographic approach. Finally, the ordering temperatures of the constituting phases were determined by means of in-situ neutron diffraction experiments.

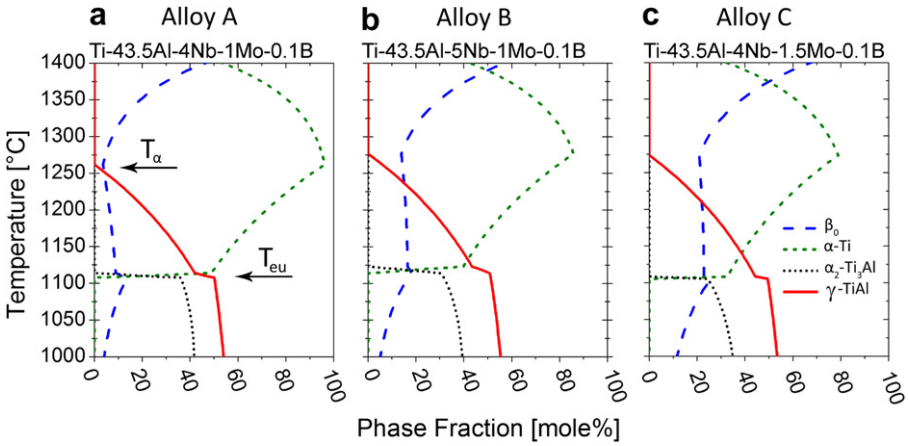

Fig. 1. Calculated phase fractions as a function of temperature for three alloys, termed A, B, and C, exhibiting different amounts of β/$β_0$ stabilizing alloying elements and 450 mass ppm O. The simulations were performed with the ThermoCalc software using a commercially available TiAl database [17]. The plotted temperature range corresponds to the range investigated by in- and ex-situ methods. T_{eu} and $T_α$ denote the eutectoid and the α-transus temperature, respectively. At T_{eu} the $α_2 \rightarrow α$ disordering reaction takes place, whereas at $T_α$ the ordered γ-phase disappears. It should be noted, that for all three alloys the predicted disordering temperature of the $β_0$-phase is above 1400 °C.

2. Material and experimental

In the present study, three different alloys were investigated which are termed A (Ti-43.5Al-4Nb-1Mo-0.1B), B (Ti-43.5Al-5Nb-1Mo-0.1B) and C (Ti-43.5Al-4Nb-1.5Mo-0.1B). Note that all chemical compositions are stated in atomic percent unless otherwise indicated. All three alloys exhibit an Al content of 43.5 at%, but different concentrations of the β/β_0 stabilizing elements Nb and Mo. Buttons with a mass of 150 g were melted in a laboratory arc-melting furnace on a water-cooled copper plate under Ar atmosphere. As starting materials, high-purity metals and Mo–Al, Al–B and Nb–Ti–Al master alloys were used [28]. Sufficient chemical homogeneity was ensured by re-melting the buttons twice. The nominal chemical composition of the alloys and the results of the chemical analyses are summarized in Table 1. For all alloys, the total amount of interstitial impurities (O, N, C, H) was smaller than 1000 wt.-ppm.

The microstructure of the three variants after solidification and after subsequent heat treatments was characterized by means of a Zeiss Evo 50 scanning electron microscope (SEM). All images were acquired in back-scattered electron (BSE) mode at an acceleration voltage of 20 kV. Details concerning the metallographic sample preparation are given in [29]. To be able to determine the β/β_0-phase content present at different temperatures, samples of the three alloys with dimensions of $10 \times 10 \times 10\ mm^3$ were heat-treated at 900 °C and 1000 °C for 6 h and at 1170, 1270 and 1350 °C for 1 h. Subsequently, the specimens were air-cooled, and metallographically examined. Image analysis with respect to the β/β_0-phase content was performed with the commercially available software package Analysis by Olympus Soft Imaging Solutions (Münster, Germany).

DSC experiments were conducted to investigate the eutectoid temperature (T_{eu}, $\alpha_2 \rightarrow \alpha$) and the α-transus temperature (T_α, γ dissolves). Both temperatures were determined for heating rates of 20 and 40 K/min and then linearly extrapolated to a heating rate of 0 K/min in order to obtain phase transition temperatures for equilibrium conditions [5]. All experiments were carried out in a dynamic Ar atmosphere with a flow rate of 50 ml/min. To account for the influence of the alumina crucibles DSC curves of the empty crucibles were subtracted from the experimentally obtained curves. The experiments were performed with a Setaram Setsys Evolution 24 instrument on specimens with a mass of approximately 40 mg.

In the in-situ HEXRD experiments the phase fractions were determined during continuous heating in an induction furnace. Details on the construction and the performance of the furnace are given in [30]. All specimens were cylinders with a diameter of 4 mm and a length of approximately 10 mm. During the experiments the furnace was flushed with Ar to reduce sample oxidation, the temperature was controlled by two pyrometers. A low temperature pyrometer was used below 650 °C, while a spectro-pyrometer with an accuracy of 0.75% was utilized for controlling the high temperature range. The specimen was rotated about its vertical axis alternating between +180° and −180° in order to improve grain statistics. Due to technical limitations it was not possible to use a thermocouple for monitoring and validating the pyrometer reading.

Table 1
Nominal and experimentally determined composition of the alloys A, B, and C. The results of X-ray fluorescence spectroscopy are given in parenthesis. All values in atomic percent.

	Alloy A	Alloy B	Alloy C
Ti	51.4 (51.77)	51.4 (50.54)	51.4 (51.04)
Al	43.5 (43.27)	43.5 (43.38)	43.5 (43.37)
Nb	4 (3.84)	5 (4.93)	4 (3.97)
Mo	1 (1.01)	1 (1.01)	1.5 (1.51)
B	0.1 (0.11)	0.1 (0.11)	0.1 (0.12)

All HEXRD experiments were performed at ID15B of the European Synchrotron Radiation Facility (ESRF) in Grenoble, France [16,25,31]. To cover the desired range of the scattering vector q a monochromatic beam with a mean energy of 86.78 keV and an energy resolution of $\Delta E/E = 10^{-3}$ was used. This energy evaluates to a wavelength λ of 0.1430 Å and a wave number k of 43.94 $Å^{-1}$. The cross-section of the primary beam at the sample position was adjusted to $0.1 \times 0.1\ mm^2$. During the experiments, the samples were heated to 1100 °C with a rate of 300 K/min, after that a 2 K/min temperature ramp was adjusted up to 1400 °C. This heating rate is a compromise between limited beam-time and insufficient counting statistics due to grain growth effects on one hand and the need to use low heating rates in order to attain phase fractions close to equilibrium conditions on the other hand.

For detecting the diffracted photons, a Thales Pixium 4700 (Thales Group, Neuilly-sur-Seine, France) area detector was used [32]. It features a resolution of 2640×1920 pixels which are $154 \times 154\ \mu m^2$ in size. To avoid overexposure of the detector while maintaining sufficient counting statistics, 12 detector images – each of 1 s exposure time – were averaged. Thus a single diffraction image with a cumulative exposure time of 12 s was generated. For data reduction and as a preliminary step for Rietveld analysis, the images were azimuthally averaged, corrected for background scattering and re-binned to a 2Θ scale. This task was performed with the software FIT2D which is described in detail in [33]. The phase fractions present at different temperatures were determined with the commercial software package Topas (Brucker AXS, Madison, WI, USA) which allows diffraction patterns to be analysed using the Rietveld method.

In-situ neutron diffraction experiments were performed to determine the temperature of the $\beta_0 \rightarrow \beta$ disordering reaction. Continuous data acquisition during heating was performed using the high intensity diffractometer WOMBAT installed at the OPAL reactor of the Australian Nuclear Science and Technology Organisation (Australia) [34].

At the two-axes powder diffractometer WOMBAT, a Ge 115 monochromator at 100° takeoff angle was used to obtain neutrons with a mean wavelength of $\lambda = 1.67$ Å, which corresponds to a wave number of $k = 3.77\ Å^{-1}$. The instrument hosts a genuine, cylindrical 2D position sensitive detector of 968×128 pixels^2 covering 120° in the scattering plane and approximately ±7.82° out of plane [33,34]. Since no detector scanning is needed, time frames only depend on the counting statistics and here a counting time of 18.2 s per frame has been chosen. For the following data evaluation, the recorded parts of the Debye–Scherrer rings were azimuthally integrated in order to obtain conventional powder diffraction patterns covering a q-range from 1 to 7 $Å^{-1}$.

Heating of the specimens was performed in an high-temperature vacuum furnace produced by AS-Scientific (Abingdon, Oxfordshire, U.K.) equipped with Nb heating filaments. The oscillating, radial collimator of WOMBAT was used to discriminate diffraction not coming from the sample position, e.g. radiation scattered by the furnace heating elements and walls [23]. From the end of the top-loading sample stick the Ø 10 mm × 50 mm sample was suspended and the temperature was measured ~15 mm from one of its ends. In the specimen chamber a pressure of less than 1.34×10^{-4} mbar was attained. Two samples have been subjected to the same heating cycle to ensure the reproducibility of the results.

3. X-ray and neutron diffraction

Despite the fact that HEXRD and neutron diffraction experiments are based on the same principle they exhibit some

pronounced differences. These stem in part from the limitations that are imposed by the corresponding radiation sources in terms of brilliance and beam size, but also from the different interactions of neutrons and photons with matter. As a first analysis step, the diffraction patterns were calibrated and the scattering angles in 2Θ were converted to positions in reciprocal space which are denoted by the scattering vector q. The length of the scattering vector q is given by

$$q = |\mathbf{q}| = (2k)\sin(\Theta) = (4\pi/\lambda)\sin(\Theta) \quad (1)$$

and is also referred to as 'momentum transfer'.

Neutrons and X-rays have different scattering contrasts, which are described by their scattering lengths b_c and $r_e \cdot f(q)$, respectively. Here b_c denotes the bound coherent neutron scattering length, which is strongly dependent on the kinds of nuclear isotopes present [35,36], r_e is the classical electron radius and $f(q)$ the so called atomic X-ray form factor which scales with the number of electrons in an atom at $q = 0$ and decreases asymptotically to 0 with increasing q values, depending on the electronic charge distribution around the nucleus. In the case of titanium aluminides, HEXRD and neutron diffraction are complementary methods. For X-rays, Ti and Al, with atomic numbers 22 and 13 respectively, both exhibit positive scattering lengths ($(r_e \cdot f)_{Al} = 3.664$ fm, $(r_e \cdot f)_{Ti} = 6.207$ fm). On the other hand for neutrons, Ti and Al have scattering lengths, b_c, that are of almost the same absolute value but have opposite signs: $b_{c,Al} = 3.449$ fm, $b_{c,Ti} = -3.370$ fm [35].

For a random solid solution, such as the atomically disordered Ti–Al phases, a virtual atom with its scattering length equal to the weighted average of the scattering lengths of the constituents is used when calculating structure factors (F, see below). While for X-rays the weighted average scattering length is a large positive number, it is close to zero for neutrons:

$$b_{c,TiAl} = b_{c,Ti} + b_{c,Al} = -3.370\,\text{fm} + 3.449\,\text{fm} = 0.079\,\text{fm}. \quad (2)$$

For any crystal, the intensity determining structure factors are the sum of the atomic scattering lengths weighted by an individual phase factor given by the position of the corresponding atom in the unit cell. If the unit cell contains several atoms, the individual atomic scattering lengths directly add up for the main reflections because in this case the phase factors are close to one. This yields high structure factors for X-ray diffraction and small ones for neutron diffraction. For some reflections, the phase factors attain values that are equal but of opposite sign due to the symmetry of the unit cell. For atomically disordered crystals, this results in reflections with zero intensity, e.g. for the 100 reflection of the disordered β-phase $b_{c,1} = b_{c,2}$ and thus $F = (b_{c,1} - b_{c,2}) = 0$. In contrast to that, for an ordered crystal these so-called superstructure peaks might attain finite intensities, since for β_0–100, $b_{c,1} \neq b_{c,2}$ the structure factor attains large absolute values for neutrons:

$$F = b_{c,Al} - b_{c,Ti} = 3.449\,\text{fm} - (-3.370\,\text{fm}) = 6.819\,\text{fm}. \quad (3)$$

If performed for X-rays, this calculation yields rather small structure factors. Thus, for disordered phases present in the Ti–Al system, X-rays produce strong main reflections, whereas almost no intensity is observed in neutron diffraction. In case of ordered phases, weak superstructure reflections appear in addition to the main reflections for X-ray diffraction, while only the strong superstructure reflections are visible for neutrons. Due to this characteristic behaviour, neutron diffraction is an ideal method for investigating order/disorder transitions in the Ti–Al system [23]. Alloying elements such as Nb ($b_{c,Nb} = 7.054$ fm) and Mo ($b_{c,Mo} = 6.715$ fm) [35] exhibit large scattering lengths and may therefore alter this behaviour. The sensitivity to order in neutron scattering experiments remains high nonetheless. On the contrary, HEXRD experiments are better suited for determining the overall phase fractions.

Quantitative evaluation of the scattering patterns acquired by HEXRD experiments was carried out by means of the Rietveld method, which allows a whole-pattern fit to be performed and thereby uses all the information contained in the diffraction patterns [37].

4. Results

Fig. 2 shows SEM micrographs taken in BSE mode from the arc-melted alloy buttons. The microstructure consists of lamellar γ/α_2-colonies which are separated by the brightly appearing β_0-phase. The microstructural features clearly indicate that solidification proceeded via the β-phase, i.e. $L \rightarrow L + \beta \rightarrow \beta \rightarrow \ldots$, followed by a multitude of solid-state transformations and reactions as described in [4]. Due to the high cooling rate the γ/α_2-lamellae cannot be resolved at the magnification used. The microstructure is fine grained with an average size of the lamellar colonies in the order of 30–60 μm and does not seem to depend on the level of β/β_0-stabilization.

A close look at the morphology of the β_0-phase evidences the presence of lens-shaped γ-phase grains, which are the product of a $\beta/\beta_0 \rightarrow \gamma$ solid-state transformation bringing the phase fractions closer to equilibrium. While the phase arrangement and grain size of the three investigated alloys are comparable, Fig. 2 reveals that the β_0-phase fraction depends on the content of Nb and Mo. Whereas alloy A (Ti-43.5Al-4Nb-1Mo-0.1B) shows the lowest volume fraction of β_0-phase (Fig. 2a), alloy C (Ti-43.5Al-4Nb-1.5Mo-0.1B) exhibits the highest amount (Fig. 2c). The β_0-phase fraction of alloy B (Ti-43.5Al-5Nb-1Mo-0.1B) lies between alloys A and C (Fig. 2b). It should be noted that the experimentally observed trend is also predicted by the ThermoCalc simulations shown in Fig. 1.

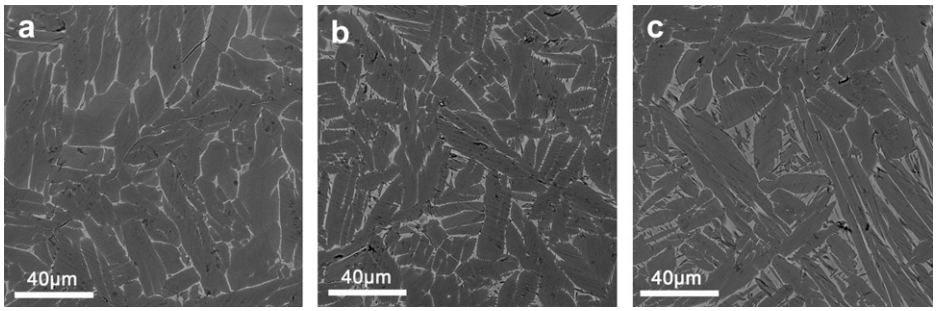

Fig. 2. Microstructure of the arc-melted alloy buttons: a) Ti-43.5Al-4Nb-1Mo-0.1B (alloy A), b) Ti-43.5Al-5Nb-1Mo-0.1B (alloy B) and c) Ti-43.5Al-4Nb-1.5Mo-0.1B (alloy C). SEM images were taken in BSE mode, i.e. lamellar γ/α_2-colonies appear grey, γ-grains dark and β_0 exhibits the brightest contrast.

A classic ex-situ approach was used to study the phases prevailing at different temperatures: samples of all three alloys were annealed in the temperature range from 900 to 1350 °C. After a certain annealing time, the samples were air-cooled which occurred with cooling rates sufficiently high for preserving the high temperature microstructure [14]. Fig. 3a–c shows the microstructure of alloy A after annealing for 1 h at 1170 °C, 1270 °C and 1350 °C, respectively. The microstructure of the sample annealed at 1170 °C is an assembly of lamellar γ/α_2-colonies with an average grain size below 40 μm and a mixture of γ and β_0-grains essentially situated at colony boundaries (Fig. 3a). According to Fig. 1a the annealing treatment at 1170 °C was conducted in the $(\alpha+\beta_0+\gamma)$ phase region.

Fig. 3b shows the microstructure after annealing at 1270 °C for 1 h and subsequent air-cooling. The temperature was selected to be slightly above T_α of the alloy which is close to the β-phase minimum (Fig. 1a). As expected, the γ-phase disappeared and the microstructure at room temperature consists of α_2 and β_0-grains.

Increasing the annealing temperature to 1350 °C leads to higher β/β_0-phase fractions (Fig. 3c) which is consistent with the predictions of the thermodynamical calculations (Fig. 1a). The micrograph obtained at room-temperature evidences the presence of fine-scaled α_2 needles within the β_0 grains. It is presumed that those precipitated during air-cooling. Quantitative analyses of the phase fractions have revealed that the sample annealed at 1270 °C shows the lowest β/β_0-phase content. The β/β_0 volume fraction of the sample heat treated at 1170 °C is slightly higher, whereas the material annealed at 1350 °C exhibits the highest fraction (see below for the specific results for all alloys).

DSC measurements were conducted on the three alloys to determine both T_{eu} and T_α. As described in section 2, two heating rates have been used and the results were linearly extrapolated to 0 K/min in order to achieve equilibrium values for T_{eu} and T_α [5]. The results of the DSC experiments are summarized in Table 2.

The results obtained from HEXRD experiments, conducted on alloy A, B, and C, are summarized in Fig. 4. Here, the phase fractions of α/α_2, β/β_0 and γ are displayed as a function of temperature. During the continuous heating experiments, the temperature was controlled by means of a high temperature pyrometer. However, the comparison of the eutectoid temperatures derived from HEXRD experiments with those obtained from DSC (Table 2) revealed that the temperature indicated by the pyrometer was erroneous.

This is attributed to the formation of an oxide layer on the sample surface during the diffraction experiments. Previous DSC and neutron diffraction studies [23] have shown that T_{eu} hardly depends on the heating rate [5,12,23]. Therefore, T_{eu} was chosen as a reference point for correcting the temperature obtained during the HEXRD experiments. This was achieved by calculating the difference between T_{eu} determined by DSC and T_{eu} gained from diffraction data first. In the next step, all temperature values recorded during the HEXRD experiment were corrected by this offset. For determining T_{eu} from diffraction data, the intensity of an α_2 superstructure peak was plotted as a function of temperature. Vanishing of the intensity indicates the loss of order and, therefore, marks T_{eu}.

In Fig. 4 the eutectoid temperature is indicated by a local maximum in the β/β_0 phase fraction and by a sudden change in the slope of the α/α_2 and γ phase fraction curves. A minimum in β/β_0 phase fraction occurs at the α-transus temperature. Accordingly, at this temperature the γ-phase vanishes. For all investigated alloys, the α-transus temperatures evaluated by HEXRD are given in Table 2.

Fig. 5 shows the course of the β/β_0-phase fraction as a function of temperature for the three investigated alloys in greater detail. Error bars of the in-situ HEXRD experiments represent the standard deviation of different Rietveld-fits. For all three alloys a minimum in β/β_0 phase fraction in the range from 1250 °C to 1300 °C can be observed which is in accordance with the results from the thermodynamic calculations shown in Fig. 1. At all temperatures alloy A exhibits the lowest β/β_0-phase content followed by alloy B, and as expected, alloy C shows the highest β/β_0-phase fractions. The solid symbols indicate the results obtained from quantitative metallography conducted on heat treated and air cooled samples as shown in Fig. 3.

The time evolution of the neutron diffraction patterns obtained during a continuous in-situ temperature ramp on WOMBAT are shown in Fig. 6. It can be seen that reflections of the ordered phases α_2, β_0, and γ disappear upon heating. At T_{eu} α_2 disorders to α, T_0 marks the loss of order in the β_0-phase and at T_α the γ-phase disappears. Although it is evident from Figs. 4 and 5 that crystalline α and β-phase is still present above T_α, no Bragg reflections are observed due to the peculiar average of the neutron scattering lengths for this material (see section 3). Instead, some diffuse scattering persists peaking at the positions of the superstructure reflections.

For alloy A the experimentally determined intensity values of superstructure peaks are plotted versus temperature in Fig. 7. The plotted intensities were gained from integration of a Gaussian fitted to the corresponding reflection-peak at a certain temperature. All integrated intensities given are background corrected. At a heating rate of 10 K/min, the reflections vanish at 1174 °C (T_{eu}), 1225 °C (T_0) and 1286 °C (T_α) for α_2, β_0, γ, respectively (Table 3). After the phase transformation, the peak intensity is close to zero and the algorithm is no longer able to perform the fit. Therefore no intensity values are given after the phase transformation has occurred. A comparison of T_α obtained by different experimental techniques

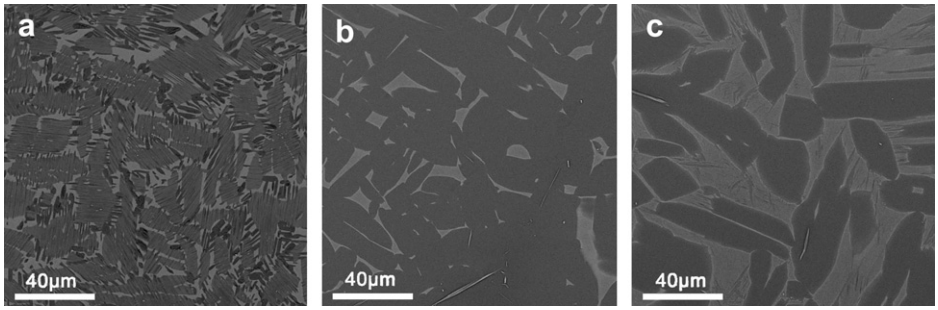

Fig. 3. Microstructure of alloy A (Ti-43.5Al-4Nb-1Mo-0.1B) after annealing at different temperatures for 1 h and subsequent air cooling: a) 1170 °C, annealing conducted in the $(\alpha+\beta+\gamma)$ phase field region; b) 1270 °C, annealing conducted in the $(\alpha+\beta)$ phase field region, close to the minimum of the β-phase (see Fig. 1a); c) 1350 °C, annealing conducted in the $(\alpha+\beta)$ phase field region.

Table 2
Transformation temperatures T_{eu} and T_{α} as determined from DSC and HEXRD experiments. Since T_{eu} was used as reference point for the temperature correction in the HEXRD experiments, the corresponding values were omitted. HEXRD experiments were conducted with a heating rate of 2 K/min. Error bars were evaluated based on the accuracy of the measured temperature and the repeatability of different analysis attempts, whereas the error of the HEXRD measurement was estimated from the accuracy of the pyrometer.

	Alloy A		Alloy B		Alloy C	
	Ti-43.5Al-4Nb-1Mo-0.1B		Ti-43.5Al-5Nb-1Mo-0.1B		Ti-43.5Al-4Nb-1.5Mo-0.1B	
	DSC	HEXRD	DSC	HEXRD	DSC	HEXRD
T_{eu} [°C]	1173 ± 5	–	1180 ± 5	–	1187 ± 5	–
T_{α} [°C]	1247 ± 5	1267 ± 9.5	1254 ± 5	1262 ± 9.5	1246 ± 5	1277 ± 9.6

shows that the results differ significantly. The reason for this behaviour is that disordering reactions as well as phase transitions require some time to occur while the temperature is constantly increased during continuous heating. Hence, the magnitude of the shift between a transition temperature determined under equilibrium conditions and one that was obtained on heating is a function of the heating rate as well as the kinetics of the phase transition as explained in the next section.

5. Discussion

The main task of this investigation is to evaluate the accuracy of the thermodynamic predictions shown in Fig. 1 [38]. From the DSC results (Table 2) it is evident that T_{eu} of the three investigated alloys is significantly higher than the ThermoCalc predictions (Fig. 1). This result is in accordance with the observations reported in [21]. A similar result was found for Ti-45Al-(5-10)Nb alloys published in [5]. The conclusion drawn from these results is that Nb and Mo act not only as β/β_0-stabilizing alloying additions, but also stabilize the ordered α_2-phase. Increasing values for T_{eu} (Table 2) as well as increasing β/β_0-phase fractions (Fig. 5) from alloy A to alloy C support this assumption. In principle, the eutectoid temperature can be determined by DSC, HEXRD and neutron diffraction experiments. Since the temperature measurement with a pyrometer was impaired during the HEXRD experiment, the eutectoid temperature determined by DSC was used as a reference point for the correction of the pyrometer reading. HEXRD experiments were conducted at heating rates of 2 K/min, for neutron diffraction a heating rate of 10 K/min was employed.

By thermodynamic calculations T_{α} was predicted to be 1260 °C for alloy A and 1275 °C for alloys B and C. In the DSC experiments (Table 2) slightly lower values for T_{α} were determined, whereas the results from HEXRD were close to the predicted values (Fig. 4). T_{α} as determined by neutron diffraction experiments on alloy A was 1286 °C (Table 3, Fig. 7). The observed differences can be explained by the sensitivity of T_{α} to the applied heating rate. In contrast to that, T_{eu} shows only a weak dependence on heating rate, which is attributed to the different natures of the occurring phase transformations. While at T_{eu} the $\alpha_2 \rightarrow \alpha$ disordering reaction takes place which requires only short-range diffusional jumps, the phase transition at T_{α} ($\gamma \rightarrow \alpha$) requires a change in crystal structure. This necessitates a collective rearrangement of whole lattice planes by changing their stacking sequence, accompanied by long-range diffusion processes to homogenize the concentration between the disappearing and prevailing phases. Therefore, this phase transition is much slower in terms of transformation kinetics, which in turn explains the higher sensitivity to the heating rate. The observed large difference in rate dependencies of T_{eu} and T_{α} has also been shown in [39]. As reported in [23] the same effect occurs upon cooling with the only difference being that the temperature shift of T_{α} is larger.

Whereas the predicted and experimentally observed transition temperatures deviate significantly for T_{eu} and moderately for T_{α} the experimentally determined course of phase fractions (Fig. 4) is similar to the result of the thermodynamic calculation (Fig. 1). Furthermore, the calculated as well as the experimentally acquired phase fraction diagrams show that an increased content of Nb and Mo shifts the minimum in β/β_0-phase fraction to larger values. The evolution of β/β_0-phase with temperature is important for wrought processing and the design of heat treatments: a high β-phase content is necessary for hot-working [4], but detrimental to the creep strength at service temperature. From Figs. 1 and 4 it is evident that alloy A shows the lowest minimum, thus rendering this specific alloy composition particularly interesting for thermomechanical processing and subsequent heat treatments. These heat treatments are conducted to minimize the β/β_0-phase fraction and to adjust a microstructure that possesses balanced mechanical properties. Usually, the heat treatment is performed in a two step fashion, in which the first step is performed close to T_{α} to reduce the amount of β/β_0-phase while the second step is a stabilization treatment conducted below 1000 °C [4,7,14].

In Fig. 5 the β/β_0-phase fraction obtained by HEXRD experiments is compared with data gained from ex-situ investigations. At 1170 °C the β_0-phase fractions obtained by HEXRD are slightly

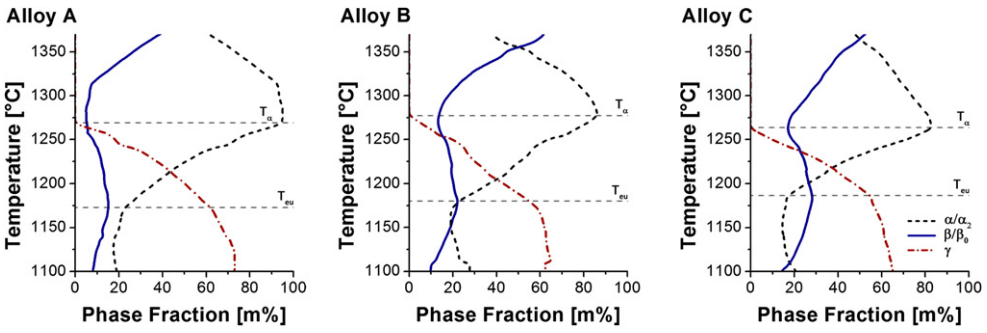

Fig. 4. Phase fractions of α/α_2, β/β_0 and γ as a function of temperature. The phase fractions were evaluated by Rietveld analysis of the corresponding HEXRD patterns. All temperature values shown were corrected by comparison with DSC measurements. The HEXRD experiments were conducted with a heating rate of 2 K/min.

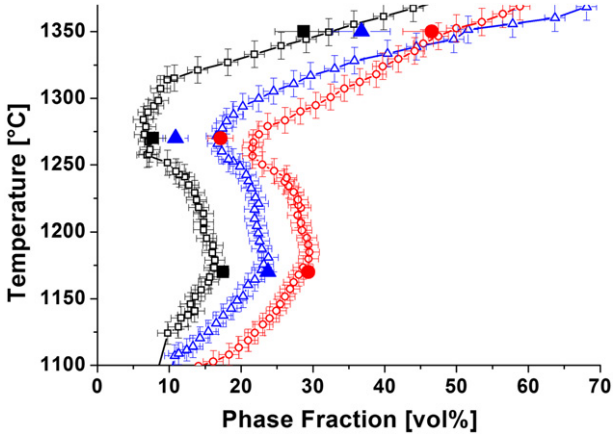

Fig. 5. β/β_0-phase fractions determined by in- and ex-situ methods. The in-situ HEXRD results of alloys A, B and C are indicated by open squares, triangles and circles, respectively. Filled symbols represent the results of quantitative metallography conducted on specimens heat-treated for 1 h at 1170 °C, 1270 °C and 1350 °C, followed by air cooling.

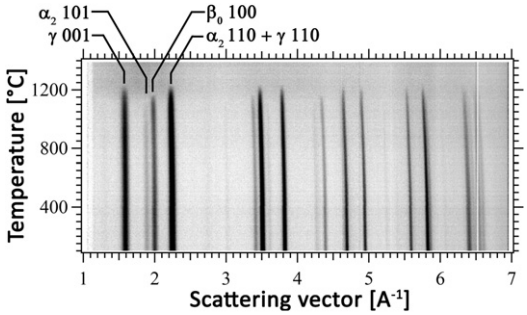

Fig. 6. In-situ neutron diffraction patterns obtained on Ti-43.5Al-4Nb-1Mo-0.1B (alloy A) (in at%) while undergoing a continuous heating ramp of 10 K/min. The intensity is coded in grey scale with black corresponding to high intensities. Reflections between $q = 1.6$ and 2.3 $Å^{-1}$ were used to establish Fig. 7.

smaller than those from quantitative metallography. This can be explained by the slow transformation behaviour of the β/β_0-phase [21] and the shorter periods of time the material has to reach equilibrium conditions during the HEXRD experiment. At 1270 °C the HEXRD and ex-situ results coincide for alloy A, but not for alloys B and C. One reason for the deviation is that the error in phase fraction determined by quantitative metallography increases with temperature. Especially for the microstructure obtained after annealing at 1350 °C the determination of the β_0-phase content is impaired by the formation of α-needles in β_0-grains which is suspected to occur during air cooling. In addition to that the quality of the HEXRD patterns diminishes with increasing temperature due to grain coarsening which decreases counting statistics. Thus, it is concluded that the observed difference between the in- and ex-situ methods used in this study can be attributed to their limited accuracy as well as to the slow transformation kinetics of the β/β_0-phase.

The deviation observed between the calculated and the experimentally determined phase fraction diagram can be attributed to the insufficient thermodynamical database for alloys with high contents of β/β_0-stabilizing elements [5,17,20,21]. Additional complications arise from the sluggish dissolution behaviour of the Nb- and Mo-rich β/β_0-phase. This is emphasized by the fact that no single α-phase region was found in the present investigations although its existence has been reported for alloys with Al contents higher than 42 at%. Clemens et al. [21] have shown that the phase fractions occurring at a certain temperature depend strongly on the annealing time which was attributed to the slow dissolution kinetics of the β-phase. Under equilibrium conditions the following solidification and transformation pathway was proposed: $L \rightarrow L+\beta \rightarrow \beta \rightarrow \beta+\alpha \rightarrow \alpha \rightarrow \alpha+\gamma \rightarrow \alpha+\gamma+\beta_0 \rightarrow \alpha_2+\gamma+\beta_0$. Continuous heating experiments performed with technically relevant heating rates, like in our in-situ HEXRD experiments, show a different behaviour as reflected in Figs. 4 and 5. Evidently, no α single phase field can be observed. Therefore, it is concluded that a heating rate of 2 K/min is not sufficiently low to enter the α single phase field. Consequently, for continuous cooling with moderate to high cooling rates as well as for isothermal short-term heat treatments the following transformation sequence is proposed: $L \rightarrow L+\beta \rightarrow \beta \rightarrow \beta+\alpha \rightarrow \alpha \ (+\beta_m) \rightarrow \alpha+\gamma \ (+\beta_m) \rightarrow \alpha+\gamma+\beta_0 \rightarrow \alpha_2+\gamma+\beta_0$, where β_m denotes the metastable β-phase. It is interesting to note that in case of the investigated alloys the thermodynamic calculation seems to describe a metastable phase behaviour rather than a behaviour expected in thermodynamic equilibrium.

In-situ neutron diffraction experiments were conducted during continuous heating on alloy A (Ti-43 Al-4 Nb-1 Mo-0.1 B) in order to study the two occurring order-disorder reactions: α_2 ($D0_{19}$) ↔ α (hcp) and β_0 (B2) ↔ β (bcc). From Figs. 6 and 7 it is evident that the disordering of the α_2-phase takes place at 1174 °C which is in good agreement with the eutectoid temperature determined by DSC experiments (Table 1).

Thermodynamic calculations predict that the order-disorder reaction $\beta_0 \leftrightarrow \beta$ takes place at a temperature of about 1420 °C [4], contradicting the good workability found at considerably lower hot-working temperatures [6,7]. Again, from Figs. 6 and 7 it is obvious that the database used does not predict the ordering

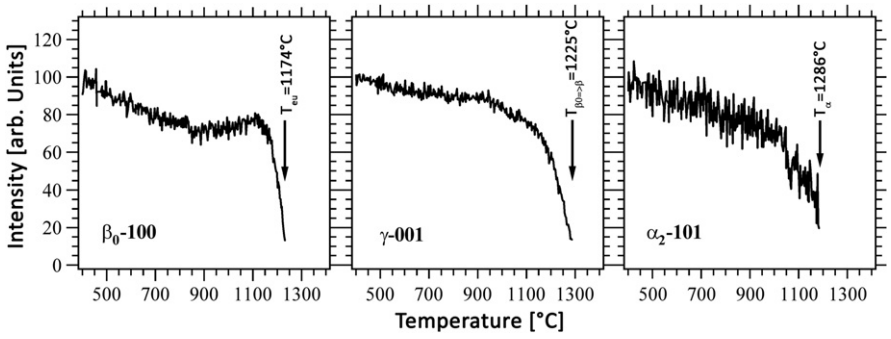

Fig. 7. Intensity evolution of the first three reflections of Fig. 6, normalized to their starting intensity at room temperature. Loss of order in one phase is indicated by a sharp drop in intensity of the corresponding reflection. The intensities do not attain zero values because some background and diffuse scattering persists.

Table 3
Order to disorder transition temperatures of alloy A (Ti-43.5Al-4Nb-1Mo-0.1B) determined by neutron-diffraction. A heating rate of 10 K/min was adjusted in the experiment.

	Alloy A
	Ti-43.5Al-4Nb-1Mo-0.1B
T_{eu} [°C]	1174
$\beta_0 \rightarrow \beta$ [°C]	1225
T_α [°C]	1286

temperature correctly. The neutron diffraction experiments show clearly that ordering occurs at about 1224 °C, which is far below the predicted value.

6. Conclusions

Three different γ-TiAl alloy variants were investigated to determine the influence of β/β_0-stabilizing elements on the prevailing phase fractions and transition temperatures. Both experiment and thermodynamic calculation with a commercial database show that an increase in Mo or Nb content increases the β/β_0-phase fraction as well as the eutectoid temperature. It has been shown that the predicted (ThermoCalc) and experimentally determined (in-situ HEXRD) evolution of phase fractions with temperature are in good agreement.

To prove the consistency of the HEXRD results, ex-situ experiments in which the samples were examined metallographically were carried out. From comparison with earlier work it is concluded that the heating rate at which the in-situ HEXRD experiments were carried out (2 K/min) is too high to obtain phase fractions that correspond to equilibrium conditions. This is highlighted by the fact, that no single α-phase field region was detected during the HEXRD experiments.

The measured phase transition temperatures deviate significantly from the ones predicted by ThermoCalc. It is shown, that T_α exhibits a rather strong dependence on heating rate which is in vivid contrast to the behaviour of T_{eu}. Temperatures of the ordering reactions were determined by in-situ neutron diffraction experiments which are particularly sensitive to atomic order in the Ti-Al system. It was thereby shown that the disordering temperature of β_0 is far below the value predicted by ThermoCalc. Upon heating with 2 K/min, the correct sequence of disordering is $\alpha_2 \rightarrow \alpha$ at T_{eu}, followed by $\beta_0 \rightarrow \beta$ before γ disappears at T_α.

Acknowledgements

Part of this research project has been supported by the European Commission under the 7th Framework Programme through the 'Research Infrastructures' action of the 'Capacities' Programme, Contract No: CP-CSA_INFRA-2008-1.1.1 Number 226507-NMI3 and by the Styrian Materials Cluster, Austria. Kun Yan contributed to the successful conduction of neutron scattering experiments which is gratefully acknowledged. In addition, the authors thank Volker Güther, GfE Metalle und Materialien GmbH, Nuremberg, Germany for fruitful discussions and preparation of the alloys.

References

[1] Kestler H, Clemens H. Production, processing and applications of gamma-TiAl based alloys. In: Leyens C, Peters M, editors. Titanium and titanium alloys. Weinheim, Germany: WILEY-VCH; 2003. p. 351–92.
[2] Wu X. Review of alloy and process development of TiAl alloys. Intermetallics 2006;14:1114–22.
[3] Yamaguchi M, Inui H, Ito K. High-temperature structural intermetallics. Acta Materialia 2000;48:307–22.
[4] Clemens H, Wallgram W, Kremmer S, Güther V, Otto A, Bartels A. Design of novel β-solidifying TiAl alloys with adjustable β/B2-phase fraction and excellent hot-workability. Adv Eng Mater 2008;10.
[5] Chladil HF, Clemens H, Zickler GA, Takeyama M, Kozeschnik E, Bartels A, et al. Experimental studies and thermodynamic simulation of phase transformations in high Nb containing γ-TiAl based alloys. Int J Mater Res 2007;98:1131–7.
[6] Kremmer S, Chladil H, Clemens H, Otto A, Güther V. Near conventional forging of titanium aluminides. In: Niinomi M, Akiyama S, Ikeda M, Hagiwari M, Maruyama K, editors. Ti-2007 science and technology. Sendai, Japan: The Japan Institute of Metals (JIM); 2008. p. 989–92.
[7] Wallgram W, Schmoelzer T, Cha L, Das G, Güther V, Clemens H. Technology and mechanical properties of advanced γ-TiAl based alloys. Int J Mater Res 2009;100:1021–30.
[8] Grujicic M, Zhang Y. Combined atomistic-crystal plasticity analysis of the effect of beta phase precipitates on deformation and fracture of lamellar $\gamma + \alpha_2$ titanium aluminide. J Mater Sci 1999;34:1419–37.
[9] Liss KD, Schmoelzer T, Yan K, Reid M, Peel M, Dippenaar R, et al. In situ study of dynamic recrystallization and hot deformation behavior of a multiphase titanium aluminide alloy. J Appl Phys 2009;106.
[10] Tetsui T, Shindo K, Kaji S, Kobayashi S, Takeyama M. Fabrication of TiAl components by means of hot forging and machining. Intermetallics 2005;13:971–8.
[11] Appel F, Paul JDH, Oehring M, Fröbel U, Lorenz U. Creep behavior of TiAl alloys with enhanced high-temperature capability. Metal Mater Trans A Phys Metal Mater Sci 2003;34 A:2149–64.
[12] Clemens H, Chladil HF, Wallgram W, Böck B, Kremmer S, Otto A, et al. A β-stabilized γ-TiAl based alloy for improved processing performance. In: New Orleans, LA, 2008, pp. 217–28.
[13] Sun FS, Cao CX, Kim SE, Lee YT, Yan MG. Alloying mechanism of beta stabilizers in a TiAl alloy. Metal Mater Trans A Phys Metal Mater Sci 2001;32:1573–89.
[14] Droessler LM, Schmoelzer T, Wallgram W, Cha L, Das G, Clemens H. Microstructure and tensile ductility of a Ti-43Al-4Nb-1Mo-0.1B alloy. In: Materials Res. Soc. Symp. Proc., MRS, Warrendale; 2009. p. 121–6.
[15] Chladil H, Clemens H, Otto A, Güther V, Kremmer S, Bartels A, et al. Charakterisierung einer β-erstarrenden γ-TiAl-Basislegierung. BHM 2006;151: 356–61.
[16] Clemens H, Chladil HF, Wallgram W, Zickler GA, Gerling R, Liss KD, et al. In and ex situ investigations of the β-phase in a Nb and Mo containing γ-TiAl based alloy. Intermetallics 2008;16:827–33.
[17] Saunders N. Phase equilibria in multi-component γ-TiAl based alloys. In: Kim YW, Dimiduk DM, Loretto MH, editors. Gamma Titanium Aluminides 1999. TMS; 1999. p. 183.
[18] Imayev RM, Imayev VM, Oehring M, Appel F. Alloy design concepts for refined gamma titanium aluminide based alloys. Intermetallics 2007;15: 451–60.
[19] Takeyama M, Kobayashi S. Physical metallurgy for wrought gamma titanium aluminides: microstructure control through phase transformations. Intermetallics 2005;13:993–9.
[20] Chladil HF, Clemens H, Leitner H, Bartels A, Gerling R, Schimansky FP, et al. Phase transformations in high niobium and carbon containing γ-TiAl based alloys. Intermetallics 2006;14:1194–8.
[21] Clemens H, Boeck B, Wallgram W, Schmoelzer T, Droessler LM, Zickler GA, et al. Experimental studies and thermodynamic simulations of phase transformations in Ti-(41-45)Al-4Nb-lMo-0.1B alloys. In: Materials Res. Soc. Symp. Proc., MRS, Warrendale; 2009. p. 115–20.
[22] Shi JD, Pu Z, Zhong Z, Zou D. Improving the ductility of γ(TiAl) based alloy by introducing disordered β phase. Scripta Metal Mater 1992;27:1331–6.
[23] Watson IJ, Liss KD, Clemens H, Wallgram W, Schmoelzer T, Hansen TC, et al. In situ characterization of a Nb and Mo containing γ-TiAl based alloy using neutron diffraction and high-temperature microscopy. Adv Eng Mater 2009;11:932–7.
[24] Liss KD, Bartels A, Clemens H, Bystrzanowski S, Stark A, Buslaps T, et al. Recrystallization and phase transitions in a γ-TiAl-based alloy as observed by ex situ and in situ high-energy X-ray diffraction. Acta Materialia 2006;54: 3721–35.
[25] Liss K-D, Bartels A, Schreyer A, Clemens H. High-energy X-rays: a tool for advanced bulk investigations in materials science and physics. Textures Microstruct 2003;35:219–52.
[26] Novoselova T, Malinov S, Sha W, Zhecheva A. High-temperature synchrotron X-ray diffraction study of phases in a gamma TiAl alloy. Mater Sci Eng A 2004;371:103–12.
[27] Reimers W, Pyzalla AR, Schreyer A, Clemens H. Neutrons and synchrotron radiation. In: Engineering materials science. Weinheim, Germany: WILEY-VCH; 2008.
[28] Güther V, Otto A, Klose J, Rothe C, Clemens H, Kachler W, et al. Microstructure and corresponding tensile properties of as-cast, β-solidifying, γ-TiAl based TNM alloys. In: TMS Annual Meeting, New Orleans, CA; 2008. p. 249–56.
[29] Schnitzer R, Chladil HF, Scheu C, Clemens H, Bystrzanowski S, Bartels A, et al. The production of lamellar microstructures in intermetallic TiAl alloys and their characterisation, Herstellung lamellarer Gefügetypen in intermetallischen TiAl-Legierungen und deren Charakterisierung, 44; 2007, 430–42.

[30] Eeckhout SG, Gorges B, Barthe L, Pelosi O, Safonova O, Giuli G. A high-temperature furnace for in situ synchrotron X-ray spectroscopy under controlled atmospheric conditions. J Synchrotron Radiat 2008;15:489–94.
[31] Tschentscher T, Suortti P. Experiments with very high energy synchrotron radiation. J Synchrotron Radiat 1998;5:286–92.
[32] Daniels JE, Drakopoulos M. High-energy x-ray diffraction using the Pixium 4700 flat-panel detector. J Synchrotron Radiat 2009;16:463–8.
[33] Hammersley AP, Svensson SO, Hanfland M, Fitch AN, Häusermann D. Two-dimensional detector software: from real detector to idealised image or two-theta scan. High Pressure Res 1996;14:235–48.
[34] Studer AJ, Hagen ME, Noakes TJ. Wombat: the high-intensity powder diffractometer at the OPAL reactor. Phys B Condens Matter 2006;385–386:1013–5.
[35] Rauch H, Waschowski W. In: Dianoux A-J, Lander G, editors. Neutron data booklet. Philadelphia: Old City Publishing; 2003. p. 1–17.
[36] Sears VF. International tables for crystallography; 2006.
[37] McCusker LB, Von Dreele RB, Cox DE, Louër D, Scardi P. Rietveld refinement guidelines. J Appl Crystallogr 1999;32:36–50.
[38] Chladil H. In: Entwicklung und Charakterisierung von hoch Niob-haltigen γ-Titanaluminid Legierungen. Leoben, Austria: Department Physical Metallurgy and Materials Testing, University of Leoben; 2007.
[39] Yeoh LA, Liss KD, Bartels A, Chladil H, Avdeev M, Clemens H, et al. In situ high-energy X-ray diffraction study and quantitative phase analysis in the $\alpha+\gamma$ phase field of titanium aluminides. Scripta Mater 2007;57:1145–8.